Effective and low-cost synthesis of Sulphur modified-TiO_2 nanopowder with improved photocatalytic performances in water treatment applications.

Alessandro Galenda [1*], Francesca Visentin [2], Rosalba Gerbasi [1], Simone Battiston [1], Naida El Habra [1]

[1] CNR-ICMATE Institute of Condensed Matter Chemistry and Technologies for Energy, National Research Council, Corso Stati Uniti, 4 35127, Padova, Italy.

[2] Department of Industrial Engineering, University of Padova, via Gradenigo, 6/a 35131 Padova, Italy.

*** Corresponding Author**

Phone +39 049 8295942

Fax +39 049 8295951

Email: alessandro.galenda@cnr.it

Abstract

In the present paper, sulphur-modified titanium dioxide (S-TiO_2) is prepared as nanopowder in mixed rutile-anatase phase by an unprecedented simple, reproducible and cheap synthetic procedure, directly employing elemental sulphur powder as sulphur source. TiO_2 and several reference TiO_2 samples obtained in pure rutile or anatase phase were also prepared with nanometric size and compared to S-TiO_2 as well as Degussa P25. The prepared samples and the reference benchmark were characterised by X-Ray Diffraction (XRD), Scanning Electron Microscopy (SEM), UV-Vis Spectroscopy, Fourier Transform Infrared Spectroscopy (FT-IR), BET specific surface area and X-ray Photoelectron Spectroscopy (XPS) techniques, while their photoactivity was determined with respect to methyl red degradation as typical probe reaction. The results from the characterisation and photocatalytic measurements were discussed and inter-correlated, thus providing a complete and consistent analysis of the samples performances. The prepared sulphur modified titanium dioxide appeared as a very efficient and long-lasting photocatalyst with respect to the unmodified

TiO_2 and to the benchmark Degussa P25 (S-TiO_2 appears to be two times faster than P25) for the methyl red removal under UV lighting, also in repeated cycles.

Keywords

Sulphur modified titanium dioxide, photocatalysis, synthesis, elemental sulphur, dye degradation.

1. Introduction

The number of studies related to environmental pollution continuously increases year by year and a very wide multiplicity of remediation techniques are proposed by the researchers, as well as the employment of the wastes as raw materials for the production of added-values new compounds or energy [1,2]. Among the remediation techniques, photocatalysis and, in general, the Advanced Oxidation Processes (AOPs), enumerate an increasing number of publications [3-5]. In this kind of process, pollutants are inertized through their mineralisation to carbon dioxide (starting from organic pollutants) or to not dangerous salts (starting from inorganic pollutants) simply employing a photocatalyst and a suitable light source. A large amount of the published works concerns pure or doped titanium dioxide as photo-active material [6-10], since it is nowadays considered as the most interesting from the industrial point of view thanks to its well-known efficiency, stability, availability, and low cost. The doping element can be either a metal or a non-metal, as a function of the specific desired purpose [11]. Since titanium dioxide light absorption is limited to UV radiation (3.0 eV and 3.2 eV band gap for rutile and anatase, respectively), a large number of studies aims to extend the absorption of the compound towards the visible spectrum, thus employing a wider part of the solar spectrum for outdoor applications, or employing common halogen or fluorescent or LED lamps for indoor applications [12]. It is worth pointing out that the performance of the visible-light absorbing TiO_2-based compounds are still quite far from those under UV condition, thus indicating that a careful assessment needs to be carried out before the process planning [13]. The use of a UV-activated efficient photocatalyst, moreover, appears sometimes inevitable in those countries where the solar radiation is inadequate, such as the northern nations, especially in winter time. Moreover, in some special closed systems, the employment of UV light could be even easier and more efficient.

The applicability of a certain technology is strictly connected to the costs of its employment, starting from the cost of the chemicals (catalysts and any other involved substances) to the management costs. The catalysts, or photocatalysts are often a significant item of expenditure, since they could be made of precious elements or prepared by an expensive

synthetic routes. Titanium dioxide is a well-known low-cost material, but its doping can involve expensive doping precursors or complicated preparation procedures.

In this paper, the synthesis of sulphur-modified titanium dioxide is conceived for using the cheapest sulphur precursor, in other words the elemental sulphur, and a common titanium precursor in sol-gel synthesis (titanium (IV) tetraisopropoxide). The choice of sulphur as foreign atom is done by taking into account the acid characteristics of this element. Its incorporation into TiO_2 lattice or, at least, the TiO_2 modification toward a more acid surface can, indeed, significantly improve the photocatalytic properties [11].

In this paper, a sulphur-modified titanium dioxide in mixed rutile-anatase phase was prepared as nanopowder, characterised by means of different and complementary analytical techniques, and tested for methyl red degradation under UV radiation in the most suitable experimental conditions [14]. Several Authors discourage the employment of dyes as probe in photocatalytic tests especially when visible light is used in order to avoid misunderstandings due to indirect photocatalytic mechanisms arising from dye light absorption and subsequent electron injection in the photocatalyst [15-17]. Nevertheless, dyes are still widely used as probes [18-20] and they can still represent a common benchmark. In the present work, methyl red was employed because UV activity was investigated and the discussion about its degradation was enriched by taking into account not only the solution bleaching, but also quantifying the overall residual absorbing molecules arising from the reaction progress. Different reference compounds were also prepared in order to compare the influence of synthetic parameters and/or the effect of the sulphur presence; Degussa P25 was also used as reference. The photocatalysts were prepared, as specified, in mixed rutile/anatase phase in order to take advantage of the heterojunction presence, thus obtaining the physical separation of photoelectrons and holes pairs and then an improved photoactivity [~~15~~21, ~~16~~22].

The synthetic procedure was planned taking into account the characteristics of several synthetic approaches. Because of this reason, the synthetic route here employed can be considered as a new and innovative way for the preparation of nanosized S-TiO_2. The method, indeed, considers the direct hydrolysis of titanium precursor in acidified water in presence of elemental sulphur powder. The choice of the most suitable sulphur source is also an important topic. A large amount of S-doped TiO_2 employs thiourea as sulphur precursor [~~17~~23-~~20~~26]. Thiourea is a not very expensive chemical but it is harmful (suspected to cause cancer and damaging the unborn child) and toxic for the environment and aquatic life. Moreover, thiourea thermal degradation leads to a multiplicity of dangerous chemicals [~~21~~27]. Elemental sulphur, on the other hand, is used in several literature works [~~22~~28-~~25~~31]; it is cheaper and very less dangerous than thiourea. Moreover, a significant number of articles uses thiourea as sulphur, carbon and nitrogen multi-element source for doping [~~26~~32, ~~27~~33], while many others use it just as sulphur source, as cited above. This aspect appears ambiguous and no *ad hoc* explanation was found in literature. Finally, several other sulphur precursors such as organic (ethanedithiol or

dimethylsulfide as few examples) or inorganic (sulphuric acid) compounds are used in literature [~~28~~34-~~30~~36], but they have been not considered for the present work because of the better properties of elemental sulphur.

2. Experimental

2.1. Synthesis

The preparation of the sulphur modified titanium dioxide-based compounds and the reference compounds was carried out by adapting the procedure proposed by Wang et al. [~~31~~37], but implementing it in order to enhance the yield close to 100% (based on Ti-precursor). The Wang protocol considers the direct hydrolysis of the titanium precursor in a water-based medium with specific acid content and specific acid to titanium and water to titanium ratios, at controlled temperature. The careful monitoring of the synthetic parameters, indeed, allows us to obtain titanium dioxide in rutile and/or rutile-anatase phase with nanometric size at low temperature.

2.1.1. Materials

Titanium (IV) isopropoxide (TTIP) 97% from Sigma-Aldrich was used as titanium precursor. Nitric acid 65 % by Fluka was used as acidifying means. Sulphur sublimed, 99.5% by Janssen Chimica was employed as sulphur precursor. AEROXIDE® TiO_2 P25 from Evonik Degussa was used as reference benchmark. All the chemicals were used as received without any further purification. Employed water was always freshly distilled.

2.1.2. Preparation of the photocatalysts

In order to obtain 1.00 g of S-TiO_2 nanoparticles, 3.67 g of TTIP 97% were carefully weighed in a dropping funnel and diluted with 36.7 g of isopropyl alcohol (1:10 TTIP to isopropyl alcohol), and dropped into a round-bottomed flask containing 190 mL of distilled water, 8.6 mL of concentrated HNO_3 and 0.90 g of sulphur powder under vigorous stirring over a 1 hour period at 50°C. The molar ratio between water and TTIP and HNO_3 and TTIP were 850:1 and 10:1, respectively.

At the end of the TTIP addition, the reaction mixture was stirred at 50°C for 2 h; during this time part of titanium precursor crystallised as nanometric rutile TiO_2, as obtained by Wang. The reaction solvent was then evaporated by heating at 80°C and the remaining solid was collected, homogenised by means of mortar and pestle, dried at 60°C at reduced pressure overnight and finally calcined at 500°C for 2 h in air. The obtained white nanopowder was named S-TiO_2.

An analogous compound was prepared by means of the same synthetic procedure but without the sulphur addition, thus obtaining the reference compound named TiO_2.

In order to complete the set of reference compounds, pure rutile and anatase-enriched titanium dioxide were prepared with nanometric size following the Wang procedure. In detail, following the same protocol, rutile TiO_2 was recovered after its formation at the end of the 2 h stirring at 50°C, dried at 60° at reduced pressure and homogenised by means of mortar and pestle. The obtained white powder was named TiO_2-W1. Anatase-enriched TiO_2 was prepared in the same conditions but the hydrolysis temperature was set at 90°C. At the end of the 2 h stirring at 90°C, the obtained solid was collected, dried at 60°C at reduced pressure and homogenised by means of mortar and pestle. The obtained white powder was named TiO_2-W2.

Finally, pure rutile and pure anatase TiO_2 were also prepared by direct hydrolysis of TTIP in water at RT and subsequent thermal treatment at 850°C for 6 h and 500°C for 5 h, respectively. The samples were named r-TiO_2 and a-TiO_2 for rutile and anatase titanium dioxide, respectively.

2.2. Measurements

The synthesised samples were characterised by complementary analytical techniques. The crystallographic structure was determined by X-Ray Diffraction (XRD) performed by means of a Philips X'Pert PW 3710 powder diffractometer operating in Bragg–Brentano θ–2θ geometry mode, using Cu Kα radiation (λ = 0.154 nm, 40 kV and 30 mA). Phase identification was performed with the support of the standard 2002 ICDD database files. The relative phase amount and the crystallite dimensions were estimated by Rietveld refinement by means of the MAUD (Material Analysis Using Diffraction) software [~~32~~38].

The X-ray Photoelectron Spectroscopy (XPS) investigations were carried out with a Perkin Elmer Φ 5600 ci Multi Technique System using a standard Al anode working at 250 W as X-ray source. The spectrometer was calibrated by assuming the binding energy (BE) of the Au $4f_{7/2}$ line to be 84.0 eV with respect to the Fermi level. Both extended spectra (survey: 187.85 eV pass energy, 0.5 eV/step, 0.05 s/step) and detailed spectra (for Ti 2p, O 1s, S 2p and C 1s: 23.5 eV pass energy, 0.1 eV/step, 0.1 s/step) were collected. The standard deviation in the BE values of the XPS line is 0.10 eV. The atomic percentage, after a Shirley-type background subtraction [~~33~~39] was evaluated by using the PHI sensitivity factors [~~34~~40]. The peak positions were corrected for the charging effects by considering the C 1s peak at 285.0 eV and evaluating the BE differences.

The specific surface area (Brunauer−Emmett−Teller (BET)) were measured by N_2 physisorption at liquid nitrogen temperature using a Micromeritics ASAP 2020 apparatus. Approximately about 100 mg of catalyst, previously degassed under vacuum for 3 h at 130°C, were used for the analysis.

The IR spectra were collected in a FT-IR Thermo-Nicolet IS10 spectrophotometer accumulating 32 scans at a resolution of 4 cm^{-1}. The spectra were acquired in transmittance mode in anhydrous KBr; for each measurement, the sample was

dispersed in anhydrous KBr (sample = 1 wt. %) and pressed as a pellet. Before each measurement, the sample was kept in nitrogen flow to eliminate water traces until a stable IR spectrum was obtained.

The surface morphology of the samples was investigated by Sigma Zeiss field emission scanning electron microscope (FE-SEM) with an electron beam acceleration voltage of 5 kV. Prior to the analyses, the sample were coated with 15 nm of Pt by Emitech K575X Turbo Sputter Coater.

The photocatalytic activity with respect to the methyl red (MR) sodium salt degradation (MR sodium salt from Sigma-Aldrich) was tested in a batch cylindrical reactor as in previous work [14], where the degradation of MR was evaluated under different conditions of concentration, photocatalyst loading and pH and the most reproducible conditions were here adopted. In each experiment, 170 mL of a 15 mg/L MR sodium salt aqueous solution (prepared at pH = 2 with H_2SO_4 in distilled water) was loaded into the reactor. 95 mg of catalyst were then added to 20 mL of the same MR solution and sonicated in dark condition for 1 hour, thus allowing the powder aggregates breaking up and the adsorption equilibrium of the dye on the catalyst surface. After sonication, the catalyst suspension was joined to the 170 mL, thus obtaining a final catalyst concentration of 0.5 g/L. The experimental set-up was completed with the insertion into the reactor of the UV lamp (Helios Italquartz low pressure Hg lamp, total power 25 W; power at 254 nm 7.5 W; power density at 254 nm at 1 m 72 $\mu W/cm^2$). The solution was constantly stirred by a magnetic stirrer and maintained at 20°C by means of a thermostatic bath. The described experimental parameters have been optimised taking into account the best compromise between the dye degradation and the catalyst concentration (using Degussa P25 as reference material). The experimental set-up was also tested in absence of any catalyst in order to evaluate the effect of the simple photodegradation induced by UV radiation and the photolysis appears negligible with respect to the photocatalytic action. The UV–Vis spectrum of the MR solution was collected before and after the introduction of the catalyst. The UV lamp was then switched on and the spectra were collected after 10, 20, 30, 40, 60, 80, 100 and 120 min of UV irradiation by withdrawing the necessary amount (about 2.5 mL) using a syringe fitted with a PVDF (polyvinylidene difluoride) membrane syringe-filter (pore size 0.45 μm). The determination of the MR amount was carried out measuring the absorbance at 518 nm and using *ad hoc* built calibration curves. Moreover, the area of the region bounded by the spectrum was calculated by numerical integration and compared to the initial value in order to quantify the overall MR mineralisation with respect to the simple solution bleaching. The UV–Vis measurements were performed with a Unicam UV500 spectrophotometer operating in the absorbance mode for the photodegradation tests or in the reflectance mode (the spectra are converted and given in absorbance units) with an integration sphere for the optical characterisation of the samples.

3. Results and Discussion

3.1. Synthesis

The synthesis of TiO_2 and modified TiO_2 in pure or mixed phase was obtained by adapting the procedure proposed by Wang et al. [~~31~~37], employing TTIP and elemental sulphur powder as titanium and sulphur precursors, respectively. Several differences distinguish the present protocol from Wang's one. Indeed, the latter is mainly focused on studying and optimizing the preparation of single pure rutile phase or mixed rutile-anatase compounds in nanometric size as a function of the experimental conditions at low temperature. Despite Wang's protocol allowed the preparation of nanometric TiO_2 in a reproducible and easy way, its limit lies in the very low yield of the synthesis. The recovered product, indeed, usually does not exceed the 10-30 wt. % of its potential, thus giving a quite high amount of wasted titanium precursor.

Starting from Wang's outcomes, the synthesis was modified as follows: the protocol was followed in terms of reaction mixture composition (optimised relative amounts of TTIP, HNO_3 and water) and the temperature was set at 50°C in order to obtain pure nanometric rutile TiO_2. At the end of Wang's procedure (2 h stirred at 50°C), the reaction solvent was completely evaporated by rising up the temperature up to 80°C. Under this condition, the remaining titanium precursor was forced to precipitate as amorphous titanium oxo-hydroxo and the suspended nanometric rutile can act as a seed for its precipitation. The solid was then recovered, homogenised with mortar and pestle, dried at 60°C at reduced pressure overnight and finally calcined at 500°C for 2 h in air. The last thermal treatment aims to induce the final anatase crystallisation, thus obtaining the intimately mixed rutile-anatase titanium dioxide. The final synthesis yield approaches 100% (save the minimal drop due to residuals on reaction vessels and mortar).

The preparation of sulphur modified TiO_2 with nanometric size was carried out by employing the above described procedure with the direct addition of sulphur powder in the reaction mixture during the rutile nucleation. In this manner, indeed, the sulphur particles can act as a nucleation seed for rutile, thus guaranteeing a highly homogeneous compound. The final thermal treatment (500°C for 2h) provides the energy for the anatase phase formation and the sulphur incorporation into titanium dioxide crystal lattice and/or the surface modification by the sulphur-containing groups. Nevertheless, the amount of sulphur content in the final S-TiO_2 compound cannot be directly predicted on the basis of the amount of sulphur powder employed in the synthesis. A significant amount of sulphur, in fact, is simply oxidised by oxygen during the thermal treatment giving sulphur oxides.

The choice of the final thermal treatment appears as a critical issue. Gomathi Devi et al. [~~22~~28], indeed, specify that sulphur residual amount is gradually reduced with temperature increase, as testified by the colour disappearance (from light brown to white, from 200 to 500°C). Moreover, they suggest that sulphur content is reduced to zero if thermal

treatment is carried out at 500°C. Nevertheless, XPS investigation here performed (see below) demonstrates that sulphur is still present after the treatment.

In the present work, the temperature was set at 500°C in order to allow both a better diffusion of sulphur atoms inside titanium dioxide crystal lattice and the anatase phase formation. The effect of a lower temperature thermal treatment as well as the effect of rutile-anatase presence, on the other hand, is still under investigation.

The sulphur precursor choice is also a very important issue. A significant amount of S-doped titanium dioxide is obtained using thiourea as precursor [~~17~~23-~~20~~26] but this chemical appears non-environmental friendly and its use was here avoided. Moreover, several authors employ thiourea as carbon, sulphur and nitrogen multi-element source for obtaining N-C-S-doped TiO_2 [~~26~~32, ~~27~~33]; this feature opens an important topic with respect to those authors that synthesise their compounds namely as only S-doped using the same precursor.

In the present work, elemental sulphur powder was used because it is cheap and not harmful (just irritating). Different authors used sulphur powder as precursor for preparing S-TiO_2, nevertheless, to the best of our knowledge, it is here used directly as received for the first time. In literature, indeed, sulphur was often dissolved in organic solvents (benzene, acetone) [~~22~~28, ~~23~~29], or supplied as sulphur vapours [~~25~~31]; finally Zhang et al. [~~24~~30] employed sulphur as powder in a mechanochemical process on pre-synthesised TiO_2. In the present paper, for the first time, sulphur powder is employed both as seed for rutile nucleation and as doping element.

3.2. Characterization

The obtained samples were analysed by XRD in order to define their crystallographic properties. It is worth pointing out that the temperature and duration of the performed thermal treatments were planned and verified for obtaining the desired compounds (in terms of crystallographic phases and crystallite dimensions) under the softest possible thermal conditions.

Figure 1 resumes the collected diffractograms, while Table 1 shows the main crystallographic data. The outcomes perfectly agree with the specific synthetic procedure adopted for each sample. Concerning the thermal stability of titanium dioxide crystallographic phases, literature suggests that anatase starts to crystallise from amorphous TiO_2 at 300°C, while in the range 580-800°C the change anatase to rutile occurs [~~35~~41]. Taking into account this, the thermal treatment of r-TiO_2 was carried out at 850°C for 6h in order to obtain pure rutile, as confirmed by the XRD analysis. Moreover, the high calcination temperature also explains the largest crystallites. On the other hand, the synthesis of a-TiO_2 (carried out at 500°C for 5h) provided pure anatase with smaller crystallites. As expected, TiO_2-W1, thanks to the soft synthetic procedure, shows the lowest crystallites dimensions, while the sample TiO_2-W2 shows slightly bigger

crystallites. Concerning the TiO_2-W2 phase composition, rutile and anatase are present, but the main phase is brookite. Wang et al. [~~31~~37] did not comment in detail the presence of brookite, but it is clearly evident from the published diffraction patterns.

The crystallite size is expected to increase with temperature, and rutile crystallites are expected to be larger than anatase, as observed by Wang. The samples a-TiO_2 and TiO_2 (treated at 500°C for 5 h), indeed, show larger crystallites and large rutile domains respectively, with respect to the ones obtained by Wang's procedure. The compound S-TiO_2, nevertheless, despite the same thermal treatment, shows smaller crystallites both for rutile and anatase. This feature can be reasonably due to the presence of sulphur powder during the rutile nucleation. Sulphur can act as a nucleation seed for rutile and the availability of a huge number of nucleation centres lead to a reduced crystallite growth. Finally, no other phases are evident in S-TiO_2 sample, and no significant variations on cell parameters or peak shifts can be detected probably because of the small sulphur amount.

The optical characterisation was carried out by means of UV-Vis spectroscopy in reflectance mode. The obtained spectra are collected and showed in Figure 2, while Table 1 reports the band gap determined from the peak onset wavelength for each compound.

The spectra in Figure 2 suggest that none of the analysed compounds gives absorption in the visible range, while the main absorption occurs just below 400 nm. The corresponding band gaps (from 3.0 to 3.1 eV), indeed, agree with literature data expected for rutile, anatase and brookite TiO_2 phases (3.2, 3.0 and about 3.1 eV for anatase, rutile and brookite, respectively [~~36~~42-~~39~~45]). The obtained outcomes then suggest that the photocatalytic properties of the prepared compounds can be exploited as best as they can do by the employment of UV emitting light source.

XPS measurement was carried out on the S-TiO_2 nanopowder sample especially in order to investigate the presence and the chemical state of sulphur. The obtained results are collected in Figure 3, where the survey spectrum (Fig. 3a), and the Ti2p (Fig. 3b), $S2p_{3/2}$ (Fig 3c) and O1s (Fig. 3d) detailed spectra are showed.

The extended spectrum (Fig. 3a) confirms that no contaminating elements are present, save adventitious carbon (285.0 eV). The peak shape and position for $Ti2p_{3/2}$ and $Ti2p_{1/2}$ contributions (459.3 and 465.0 eV respectively, Fig. 3b) agrees with titanium (IV) in titanium oxide [~~40~~46]. Figure 3c clearly shows that no signals are present at about 160-161 eV (sulphur as S^{2-}) or at about 163.5-164.5 eV (sulphur as element), while the only contribution appears at about 169.3 eV. The signal appears as a single peak which is the sum of $S2p_{3/2}$ and $S2p_{1/2}$ contributions, not highlighted as single peaks because of the reduced peak splitting (about 1.2 eV) [~~24~~30]. The sulphur detailed spectrum gives important information concerning the behaviour of the element. The analysis suggests that sulphur was not included as sulphide (i.e. not

substituting for oxygen) into titanium dioxide lattice and no evidence of pristine elemental sulphur precursor is present [4046]. Literature references suggest that sulphur can accommodate both as substitute on titanium lattice sites, or as surface terminating group as sulphate [1723]. Moreover, literature also suggests that, when present as titanium (IV) substitute, sulphur can be in (IV) o (VI) oxidation state. The XPS peak position for S^{4+} or S^{6+}, indeed, are quite closed (about 168.8 and 169.5 eV for S^{4+} or S^{6+}, respectively [2531]). Sethi et al. [7], prepared S-doped TiO_2 from $TiOSO_4$ and Na_2SO_4 as sulphur source; from the XPS characterisation they concluded that sulphur was S^{4+} as Ti(IV) substitute, but no explanation concerning the S(VI) to S(IV) reduction during the synthesis were given. The results obtained in the present work agree with the literature hypotheses [7, 4147, 4248] and the observed S2p XPS contribution can be related to S^{6+} as sulphate group or S^{4+} as Ti(IV) substitute. In the last case, nevertheless, no correspondence can be found in the XRD analysis (no peak shift was observed) because of the small sulphur amount.

O1s XPS signal appears as single broad peak centred at 530.7 eV with a shoulder at about 532.4 eV. The signal can be made up of at least three components; the first one, at about 530.2 eV concerning the TiO_2 oxide lattice contribution, the second one at about 531.2 eV, related to surface hydroxyl terminations, and the last one at about 532.4 eV ascribable to sulphate/sulphite termination groups [7,1723,4248,4349].

The XPS analysis also provided the surface composition of the S-TiO_2 sample in terms of relative atomic percentage; the outcomes indicate 23% titanium, 74% oxygen, and 3% sulphur. The obtained data suggest a significant enrichment for oxygen with respect to the theoretical value for TiO_2 (i.e. 67%), which is compatible with both surface hydroxyl terminations and with sulphate groups as well as molecularly chemisorbed water. The amount of sulphur can be hardly compared to literature data since very different sulphur contents arise from different synthetic procedure (differing for sulphur sources, initial amount and thermal treatments), showing values from 0.5 to 10% [2228, 2329, 2834, 3036, 4147, 4247, 4450]. Literature generally agrees about the sulphur decrease with temperature in thermal treatment. Because of this reason, the preliminary calculation for the initial sulphur precursor content appears hard to be carried out and a post-synthesis determination is the most appropriate indication.

In order to confirm the presence of the sulphate groups, the sample S-TiO_2 was investigated by means of FT-IR spectroscopy in the range 400-4000 cm^{-1}. The sample TiO_2 was also investigated for a direct comparison and for a better highlighting of the sulphur effect on TiO_2. The strongest signal appears as a wide band between 500 and 700 cm^{-1} and is related to vibration of Ti-O-Ti bond; the peak at 1630 cm^{-1} and the wide band between 2800 and 3600 cm^{-1} are ascribable to the hydroxyls and adsorbed water molecules stretching and bending vibration modes [1723, 2228, 2935, 3036, 4349]. Thanks to the normalization of the collected spectra, the comparison between the H_2O/OH IR signals (1630 and 2800-3600 cm^{-1}) suggests that the S-doped sample shows a large amount of water/hydroxyls, as confirmed

by Gomathy-Devi et al. [~~43~~49]. This feature can be particularly significant for the photocatalytic activity of S-TiO_2, since both adsorbed water and hydroxyl groups are involved in the reactive species (radicals) formation in the photocatalysis.

FT-IR analysis also provided important information concerning the sulphur state in the S-doped TiO_2. Literature data indicate that characteristic IR signals in the range 950-1350 cm^{-1} are diagnostic for the presence of different sulphur-related species. In detail, the Ti-O-S and the S-O vibrations occur at about 1050 cm^{-1} and about 1130 cm^{-1}, respectively. Moreover, a peak at about 1340-1400 cm^{-1} seems to be characteristic for the asymmetric stretching of S=O bond in sulphate group [~~17~~23, ~~22~~28, ~~30~~36, ~~43~~49]. In the present work, the IR spectrum of S-TiO_2 shows two contributions at 1040 and 1137 cm^{-1}, but no signal at about 1400 cm^{-1}. Under this condition, Gomathi-Devi et al. [~~43~~49] suggest the presence of bidentate sulphate ions, while Han et al. [~~30~~36] confirm the presence of S-O (1130 cm^{-1}) and Ti-S (1045 cm^{-1}) bonds, and thus the incorporation of sulphur into TiO_2 matrix, but the absence of any contribution at about 1400 cm^{-1} indicates a lack of surface sulphate species. The results here obtained can also be conveniently compared with the outcomes from Nanayakkara et al. [~~45~~51] and Topalian et al. [~~46~~52] concerning the interaction between SO_2 and TiO_2. The here adopted synthetic procedure, indeed, suggests that elemental sulphur can be thermally oxidised in air to SO_2 during the calcination at 500°C for 5h and the in situ produced SO_2 can then interact with TiO_2. Thanks to Nanayakkara et al. [~~45~~51] and Topalian et al. [~~46~~52], it can be reasonably hypothesised that SO_2 can react with hydroxyl termination on TiO_2 surface, thus producing sulphite-related species (region between 800 and 1200 cm^{-1}) and adsorbed water, also resulting in a more acid surface. A more acidic surface, indeed, can lead to a better adsorption of organic substances and lengthen the lifetime of photoelectron-hole pairs [11].

The SEM analysis outcomes concerning the sample morphologies are resumed in Figure 5. At low magnification (not shown for sake of brevity), r-TiO_2 appears as a collection of irregular very large particles (between 10 and 200 μm); r-TiO_2, moreover, shows the lowest specific surface area (0.4 m^2/g – Table 1) thus confirming the effect of the high temperature thermal treatment. TiO_2-W1 (pure rutile) seems a homogeneously dispersed sub-micrometric powder. The high magnification images (Figure 5a and 5b for r-TiO_2 and TiO_2-W1, respectively) show a dense and compact agglomeration of polyhedric particles (most of them 150-300 nm wide) for r-TiO_2; TiO_2-W1, on the other hand, appears as a dispersion of nanoparticles, showing the smallest particles among the entire sample set. The BET specific area for TiO_2-W1 well agrees with the SEM images and represents the highest obtained value (143.8 m^2/g) among the sample set. Figure 5c shows the TiO_2-W2 sample morphology. With respect to TiO_2-W1, which was obtained under similar conditions (low temperature TTIP controlled hydrolysis; 50°C for TiO_2-W1, 90°C for TiO_2-W2), TiO_2-W2 shows slightly wider porous agglomerates, also confirmed by a lower BET specific area (70.6 m^2/g).

Despite the stronger thermal treatment (500°C for 5h), a-TiO_2 (Figure 5d) morphology appears quite similar to TiO_2-W2, but the particle agglomerates appear closer, thus showing a lower porosity; nevertheless the BET specific area value is slightly higher than TiO_2-W2 (83.1 vs 70.6 m^2/g). Figure 5e and 5f show the outcomes obtained for the samples TiO_2 and S-TiO_2, respectively. At low magnification (not shown), S-TiO_2 shows a higher number of smaller agglomerates with respect to TiO_2, which is consistent with the sulphur suspension particles nucleation action during the TTIP hydrolysis. At higher magnification, TiO_2 (Figure 5e) appears as a porous agglomerate made of nanoparticles, while S-TiO_2 (Figure 5f) shows a more irregular micro-and nano-morphology, with nanometric spherical particles placed over micrometric agglomerates. Finally, Figure 5g shows the P25 morphology. The appearance of P25 suggests the presence of well dispersed spherical 40-70 nm wide nanoparticles.

The obtained SEM outcomes but S-TiO_2, well agree with the expected features related to the adopted synthetic procedures both in terms of particle dimensions and particle dispersion-agglomeration, and in relation to the crystallite dimensions calculated by the Rietveld refinement (see Table 1). S-TiO_2, on the other hand, appears more compact (although nanostructures are well dispersed on the compact ones) with respect to the analogous TiO_2. The observed packed structures could be related to a local temperature increase (above the nominal 500°C), and thus causing the nanoparticles agglomeration, due to sulphur particles burning during the thermal treatment of the sample. The appearance of the samples TiO_2 and S-TiO_2 well agrees with the BET surface area obtained values: 85.8 and 123.7 m^2/g respectively. The S-TiO_2 surface area, in detail, appears significantly high, despite the 500°C thermal treatment (compared to TiO_2 and a-TiO_2), thus testifying the improvement in the sample morphology (and area) given by the sulphur presence as nucleation agent in the synthesis.

3.3. Photocatalytic tests

The synthesised samples were investigated with respect to the methyl red (MR) degradation in a photocatalytic test under UV 254 nm irradiation. Methyl red was chosen as a typical dye probe detectable in textile industry waste water. Methyl red is also considered as a probe molecule in a large number of literature articles [~~47~~18-~~49~~20], thus allowing a better comparison of the obtained results, since a new synthetic procedure is here proposed.

Previous studies [14] indicate that MR photodegradation is affected by several experimental conditions and the solution pH plays a critical role. Because of this reason, the photocatalytic tests were carried out at 20°C at pH = 2 by H_2SO_4.

Figure 6a and 6b show~~s~~ the C_i/C_0 ratio (MR concentration at the time "i" with respect to initial concentration C_0) and A_i/A_0 ratio (area bounded by the UV-Vis spectra at the time "i" with respect to initial area A_0) trends as a function of reaction time for the investigated samples. Table 2 resumes the MR conversion and total absorbing residuals after 10,

30 and 120 minutes reaction (calculated with respect to the 518 nm peak of MR UV-Vis spectrum and with respect to the area bounded by the spectra) as well as the calculated first order kinetic constant values (calculated with respect to MR disappearance).

The experimental data confirm the poor photocatalytic activity of rutile-based samples: r-TiO_2 and TiO_2-W1, indeed, appear as the worst catalysts. The sample r-TiO_2, in detail, gives the worst performance among the overall prepared samples and this feature is ascribable both to the rutile crystallographic phase, to the largest particle sizes (as testified from SEM images and crystallites dimension in Table 1) and the lowest surface area caused by the high temperature thermal treatment (850°C for 6 h). On the other hand, TiO_2-W1 shows a slightly better activity that can be related to the nanometric crystallites and the highest surface area among the prepared samples. The sample TiO_2-W2 shows a significant improvement with respect to the rutile-based compounds. The activity of TiO_2-W2, despite the lower surface area with respect to TiO_2-W1, can be related to both to the nanometric size of the crystallites and to the presence of different crystallographic phases (i.e. the heterojunction effect). Nevertheless, the preponderance of brookite appears as a drawback [~~50~~53]; the activities of brookite-free samples (TiO_2 and a-TiO_2) are indeed better than TiO_2-W2.

The photoactivity of S-modified TiO_2 nanopowder appears as the best among the investigated samples and its performance is about twice better than the benchmark Degussa P25, thus suggesting S-TiO_2 as a suitable compound for water treatment. S-TiO_2, indeed, degrades about 96% MR after 10 minutes reaction time versus 77% for P25. Table 2 resumes quantitative data concerning MR conversion and the corresponding first order kinetic constants.

The obtained outcomes confirm the very good photocatalytic properties of S-TiO_2 (k_I = 0.310 min^{-1}) with respect to P25 (k_I = 0.151 min^{-1}).

Figure 7 shows the UV-Vis spectra obtained at increasing reaction time for S-TiO_2 and Degussa P25 (i.e. the two best tested compounds). MR pre-adsorption on catalyst surface in dark conditions is more intense for S-TiO_2 (about 10%) rather than for P25 (about 4%). The substrate (MR in this case)-photocatalyst interaction is mainly due to electrostatic phenomena [~~51~~54] and the different behaviour can be related to a different surface acidity of the catalysts. As discussed in a previous work [14], the relative acid/base properties of both catalyst and dye should be taken into account. In this case, the pH was 2 for both experiments (i.e. the acid/base equilibrium for MR was driven toward net positive charge in both cases), thus it is reasonable to hypothesise that the S-TiO_2 surface has a wide number of negative charged surface groups. This hypothesis is also sustained by the presence of acid –SO_3H surface functional groups, as suggested by the FT-IR analysis (peaks at 1040 and 1137 cm^{-1}, Figure 4).

The evolution of the reaction mixture spectra as a function of reaction time indicates that S-TiO_2 allows a faster MR degradation, with a rapid bleaching (i.e. no further absorption in the visible range of the spectra) of the solution after few tens of minutes. Nevertheless, both reaction mixtures show a residual absorption in the 200-400 nm range, which

can be due to the presence of MR-related degradation fragments (see also Figure 6b). The photocatalytic oxidation process, as known, involves the formation of different high reactive species that fragment the pristine molecule (MR in this case) in a complex mixture of simpler molecules toward their complete mineralisation to carbon dioxide and water. Comparelli et al. [52~~52~~55] and Mascolo et al. [53~~53~~56] suggested a possible mechanism for MR degradation, but the detailed composition of the last degradation steps is hard to be carried out. From Mascolo's hypothesis, it can be deduced that MR degradation, after the aza-bond breakage, can produce aromatic fragments similar to benzoic acid (absorption at 220 nm), salicylic acid (absorption at 300 and lower than 250 nm) and aniline (absorption at 340 and 220 nm) related molecules. The shape of the UV-Vis spectra obtained for S-TiO_2 and P25 (Figure 7) appears very similar each other, thus suggesting that the same reaction mechanism takes place. Under this hypothesis, the presence of sulphur seems do not produce any significant modification except from the kinetic point of view (the band gaps also show very close values). Because of this reason, it seems plausible that the advantage in using S-modified TiO_2 concerns essentially in a more efficient management of the photoelectron-hole pairs, thus allowing a longer lifetime and guaranteeing their better exploitation towards the photocatalytic reaction rather than their recombination. The increased surface acidity and a larger surface area also helps in a better extraction of photoelectron from the bulk and a better interaction (i.e. better adsorption) with the methyl red molecule, respectively. Concerning the complete MR mineralisation, the outcomes showed in Figure 6b suggest that a residual absorption is still present after 120 minutes reaction time. The main information is related to the incomplete MR mineralisation, and about 10% of residual absorbing molecules are still present both for S-TiO_2 and P25. This consideration suggests that longer times are required for gaining the complete MR removal.

From environmental and industrial point of view, the reutilisation of the catalysts represents of course an undeniable advantage. Because of this reason, S-TiO_2 sample was recovered after the photocatalytic test and reused for further three cycles under the same conditions in order to evaluate its performance. S-TiO_2 was gathered by filtration through 0.45 μm PVDF filter, washed with three times with distilled water and dried in vacuum at 50°C; the catalyst recovery approaches 85% by weight after each cycle. Figure 8 shows the C_i/C_0 ratio trends as a function of reaction time for the four investigated cycles. S-TiO_2 photocatalytic property appears fundamentally preserved and the main difference is evident in the first minutes of the cycles 2, 3 and 4. In those cases, the degradation of MR appears slightly slower (about 8% residual MR versus about 4% of the first cycle). Nevertheless, the degradation trends in the cycles 2, 3 and 4 align themselves to that of the first one starting from the 20^{th} minute. It is worth pointing out that the S-TiO_2 sample recovered after the first photocatalytic test (and so after the second to fourth cycles) appeared not perfectly white, but a slight beige colour was evident. This feature could be related to residual adsorbed MR or MR related compounds, which remains adsorbed on S-TiO_2 surface, thus slowing down its photocatalytic action. Taking into account the observed

trends for the cycles 2, 3 and 4, the catalyst contamination appears to reach a steady condition after the first usage and no significant further deteriorations are evident. The results of the reutilisation tests then suggest that S-TiO_2 can be a powerful catalyst even if used in repeated water treatment cycles.

When dealing with pollutants remediation from both water and air by means of photocatalytic processes, it is necessary to provide a more insightful point of view. Most authors, beyond the C_i/C_0 ratios versus time diagrams, concerning the degradation/disappearance of the diagnostic analytical signals of the investigated pollutant, add complementary analyses such as COD (chemical oxygen demand), TOC (total organic carbon) or chromatographic determinations [47-49, 53] for testifying the pollutant mineralisation rather than the solution bleaching. Because of the difficulty and the cost rise for an accurate determination of the final composition of the reaction mixture and also taking into account that the aim of the photocatalytic process is the complete mineralisation of the pollutants, a smart tool for a fast and free of charge comparison of the effectiveness of different photocatalysts is to quantify the residual UV-Vis absorption of the reaction mixture. In the present work, the residual absorption is calculated by the numerical integration of the area of the region bounded by the spectrum. The lower this area is, the more efficient the photocatalyst will be. The photocatalytic process reaches its target when the residual area approaches to zero.

From Table 2 and Figure 6b, it can be seen that after 120 minutes reaction time, none of the catalysts completely mineralised the MR fragments and the best performance is for S-TiO_2, where about 9% of the initial amount is still not-mineralised. This suggests that, despite the high degradation of the pristine molecule, the oxidation process still needs to be optimised by a fine tuning of the reaction conditions. Concerning the repeated photocatalytic tests on S-TiO_2, the residual percentage areas are 9, 14, 8, 10 after the first, second, third and fourth cycle, respectively, thus confirming a significant stability of the investigated catalyst.

As an overview of the obtained results, sulphur doped rutile-anatase titanium dioxide appears as the best tested compound. The sulphur presence seems allowing a more extended hydroxylation of the sample surface, thus giving a large number of reactive sites for the formation of oxygen-hydroxyls-based radicals from the photo-generated electron-hole pairs and a large number of acidic sites for a stronger interaction with methyl red, furthermore the synergic presence of the rutile-anatase mixed phase seems to further improve the catalyst performance.

4. Conclusion

In this contribution a new and optimised synthetic route is proposed for the preparation of sulphur modified titanium dioxide with nanometric size in mixed rutile-anatase phase for photocatalytic applications. The preparation procedure involves the use of elemental sulphur powder as seed for rutile nucleation and the subsequent anatase precursor

precipitation, followed by the final thermal treatment. Different compounds have been prepared in order to verify the influence of different parameters (such as crystallographic phase, crystallite dimensions, modifying element presence) on the photoactivity with respect to methyl red degradation as model reaction. The obtained samples have been characterized by means of different analytical techniques such as X-ray diffraction, UV-Vis spectroscopy, Scanning Electron Microscopy, BET specific surface area, X-ray Photoelectron Spectroscopy and Fourier Transform Infrared Spectroscopy. The correlation of the obtained results allowed a deeper comprehension between the sample characteristics and the sample reactivity.

S-modified TiO_2 appears as the best investigated compound among the synthesised ones. The planned synthetic procedure, thanks to the presence of sulphur and the synergic rutile-anatase role, provides a route for a better electron-hole pairs exploitation and the enhancement of surface hydroxylation, surface acidity and obtaining higher surface area nanopowder. S-TiO_2 overtakes P25 in MR degradation, thus confirming that it can be a suitable compound for water photo-remediation. The photocatalytic performance of S-TiO_2 was also verified in four subsequent repeated cycles, thus confirming the retention of its optimal photocatalytic properties with respect to MR degradation. The methyl red degradation goodness is here evaluated taking into account both the solution bleaching (simple pristine MR molecule degradation) and the residual solution absorption for a smart and fast quantification of the pollutant mineralisation.

Acknowledgements

This work was partially funded by the European Union's Seventh Programme for research, technological development and demonstration under grant agreement No 609180, Energy efficient & Cost competitive retrofitting solutions for shopping buildings -Ecoshopping. The authors acknowledge Dr. L. Nodari for the FT-IR analyses, Dr. M.M. Natile for XPS measurements and Dr. Alberto Garbujo for BET surface analyses.

References

[1] Singh, V., Tiwari, A., Das, M., (2016). Phyco-remediation of industrial waste-water and flue gases with algal-diesel engenderment from micro-algae: a review. Fuel, 173, 90-97.

[2] Das, S., Sen, B., Debnath, N., (2015). Recent trends in nanomaterials applications in environmental monitoring and remediation. Environmental Science and Pollution Research, 22, 18333-18344.

[3] Klavarioti, M., Mantzavinos, D., Kassinos, D., (2009). Removal of residual pharmaceuticals from aqueous systems by advanced oxidation processes. Environment International, 35, 402-417.

[4] Muruganandham, M., Suri Rominder, P.S., Sillanpää, M., Wu, J.J., Bashir, A., Balachandran, S., Swaminathan, M., (2014). Recent developments in heterogeneous catalyzed environmental remediation processes. Journal of Nanoscience and Nanotechnology, 14, 1898-1910.

[5] Chong, M.N., Jin, B., Chow, C.W.K., Saint, C., (2010). Recent developments in photocatalytic water treatment technology: a review. Water Research, 44, 2997-3027.

[6] Hashimoto, K., Irie, H., Fujishima, A., (2005). TiO2 photocatalysis: a historical overview and future prospects. Japanese Journal of Applied Physics, 44, 8269-8285.

[7] Sethi, D., Pal, A., Sakthivel, R., Pandey, S., Dash, T., Das, T., Kumar, R., (2014). Water disinfection through photoactive modified titania. Journal of Photochemistry and Photobiology B: Biology, 130, 310-317.

[8] Verbrugger, S., (2015). TiO2 photocatalysis for the degradation of pollutants in gas phase: From morphological design to plasmonic enhancement. Journal of Photochemistry and Photobiology C: Photochemistry Review, 24, 64-82.

[9] Murgolo, S., Petronella, F., Ciannarella, R., Comparelli, R., Agostiano, A., Curri, M.L., Mascolo, G., (2015). UV and solar-based photocatalytic degradation of organic pollutants by nano-sized TiO2 grown on carbon nanotubes. Catalysis Today, 240, 114-124.

[10] Friedmann, D., Mendive, C., Bahnemann, D., (2010). TiO2 for water treatment: parameters affecting the kinetics and mechanisms of photocatalysis. Applied Catalysis B: Environmental, 99, 398-406.

[11] Carp, O., Huisman, C.L., Reller, A., (2004). Photoinduced reactivity of titanium dioxide. Progress in Solid State Chemistry, 32, 33-177.

[12] Etacheri, V., Di Valentin, C., Schneider, J., Bahnemann, D., Pillai, S.C., (2015). Visible-light activation of TiO2 photocatalysts: Advances in theory and experiments. Journal of Photochemistry and Photobiology C: Photochemistry Review, 25, 1-29.

[13] Paz, Y., (2010). Application of TiO_2 photocatalysis for air treatment: patents' overview. Applied Catalysis B: Environmental, 99, 448-460.

[14] Galenda, A., Crociani, L., El Habra, N., Favaro, M., Natile, M.M., Rossetto, G., (2014). Effect of reaction conditions on methyl red degradation mediated by boron and nitrogen doped TiO_2. Applied Surface Science, 314, 919-930.

[15] Rochkind, M., Pasternak, S., Paz, Y., (2015). Using dyes for evaluating photocatalytic properties: a critical review. Molecules, 20, 88-110.

[16] Shaham-Waldmann, N., Paz, Y., (2016) Away from TiO2: a critical minireview on the developing of new Photocatalysis for degradation of contaminants in water. Materials Science in Semiconductor Processing, 42, 72-80.

[17] Ohtani, B., (2014) Revisiting the original works related to titania Photocatalysis: a review of papers in the early stage of Photocatalysis studies. Electrochemistry, 82(6), 414-425.

[18] Sahoo, C., Gupta, A.K., Pal, A., (2005). Photocatalytic degradation of methyl red dye in aqueous solutions under UV irradiation using Ag^+ doped TiO2. Desalination, 181, 91-100.

[19] Badr, Y., Abd El-Wahed, M.G., Mahmoud, M.A., (2008). Photocatalytic degradation of methyl red dye by silica nanoparticles. Journal of. Hazardous Materials, 154, 245-253.

[20] Lachheb, H., Puzenat, E., Houas, A., Ksibi, M., Elakoui, E., Guillard, C., Herrmann, J.M., (2002). Photocatalytic degradation of various types of dyes (Alizarin S, Crocein OrangeG, Methyl Red, Congo Red, Methylene Blue) in water by UV-irradiated titania. Applied Catalysis B: Environmental, 39, 75-90.

[~~15~~21] Hurum, D.C., Agrios, A.G., Gray, K.A., Rajh, T., Thurnauer, M.C., (2003). Explaining the enhanced photocatalytic activity of Degussa P25 mixed-phase TiO_2 using EPR. Journal of Physical Chemistry B, 107 4545-4549.

[~~16~~22] Scanlon, D.O., Dunnill, C.W., Buckeridge, J., Shevlin, S.A., Logsdail, A.J., Woodley, S.M., Richard, C., Catlow, A., Powell, M.J., Palgrave, R.G., Parkin, I.P., Watson, G.W., Keal, T.W., Sherwood, P., Walsh, A., Sokol, A.A., (2003). Band alignment of rutile and anatase TiO_2. Nature Materials, 12, 798-801.

[~~17~~23] Abu Bakar, S., Ribeiro, C., (2016). An insight toward the photocatalytic activity of S doped 1-D TiO2 nanorods prepared via novel route: As promising platform for environmental leap. Journal of Molecular Catalysis A: Chemical., 412 78-92.

[~~18~~24] Yan, C., Yi, W., Yuan, H., Wu, X., Li, F., (2013). A highly photoactive S, Cu-codoped nano-TiO_2 photocatalyst: synthesis and characterization for enhanced photocatalytic degradation of neutral red. Environmental Progress and Sustainable Energy, 33, 419-429.

[~~19~~25] Li, W., Yan, C., Yan, P., Li, F., (2014). A new perspective for effect of S and Cu on the photocatalytic activity of S, Cu-codoped nano-TiO_2 under visible light irradiation. Journal of Sol-Gel Science and Technology, 69, 386-396.

[~~20~~26] Feilizaded, M., Vassoughi, M., Zakeri, S.M.E., Rahimi, M., (2014). Enhancement of Efficient Ag-S/TiO_2 nanophotocatalyst for photocatalytic degradation under visible light. Industrial and Engineering Chemistry Research, 53, 9578-9586.

[~~21~~27] Zerong, D.W., Motoko, Y., Ben, G., (2013). Theoretical study on the thermal decomposition of thiourea. Computational and Theoretical Chemistry, 1017, 91-98.

[~~22~~28] Gomathi Devi, L., Kavitha, R., Nagaraj, B., (2015). Bulk and surface modification ofTiO2 with sulfur and silver: synergetic effects of dual surface modification in the enhancement of photocatalytic activity. Material Science in Semiconductor Processing, 40, 832-839.

[~~23~~29] Xu, P., Xu, T., Lu, J., Gao, S., Hosmane, N.S., Huang, B., Dai, Y., Wang, Y., (2010). Visible-light-driven photocatalytic S- and C- codoped meso/nanoporous TiO2. Energy Environmental Science, 3, 1128-1134.

[~~24~~20] Zhang, Q., Wang, J., Yin, S., Sato, T., Saito, F., (2004). Synthesis of a Visible-Light Active TiO2_xSx Photocatalyst by means of mechanochemical doping. Journal of American Ceramic Society, 87, 1161-1163.

[~~25~~31] Ni, J.; Fu, S.; Wu, C.; Maier, J.; Yu, Y.; Li, L., (2016). Self-supported nanotube arrays of sulfur-doped TiO2 enabling ultrastable and robust sodium storage. Advanced Materials, 28, 2259-2265.

[~~26~~32] Lei, X.F., Xue, X.X., Yang, H., Chen, C., Li, X., Niu, M.C., Gao, X.Y., Yang, Y.T., (2015). Effect of calcination temperature on the structure and visible-light photocatalytic activities of (N, S an C) co-doped TiO2 nano-materials. Applied Surface Science, 332, 172-180.

[~~27~~33] Amreetha, S., Dhanuskodi, S., Nithya, A., Jothivenkatachalam, K., (2016). Three way electron transfer of a C–N–S tri doped two-phase junction of TiO_2 nanoparticles for efficient visible light photocatalytic dye degradation. RCS Advances, 6, 7854-7863.

[~~28~~34] Scarisireanu, M., Morjan, I., Alexandrescu, R., Fleaca, C.T., Badoi, A., Dutu, E., Nicolescu, A.M., Luculescu, C., Vasile, E., Wang, J., Bouhadoun, S., Herlin-Boime, N., (2014). Enhancing the visible light absorption of titania nanoparticles by S and C doping in a single-step process. Applied Surface Science, 302, 11-18.

[~~29~~35] Sharotri, N., Sud, D., (2015). A greener approach to synthesize visible light responsive nanoporous S-doped TiO2 with enhanced photocatalytic activity. New Journal of Chemistry, 39, 2217-2223.

[~~30~~36] Han, C., Andersen, J., Likodimos, V., Falaras, P., Linkugel, J., Dionysiou, D.D., (2014). The effect of solvent in the sol-gel synthesis of visible light-activated sulfur-doped TiO2 nanostructured porous films for water treatment. Catalysis Today, 224, 132-139.

[~~31~~37] Wang, L., Yuan, Z., Egerton, T., (2012). Comparison of nano-particulate TiO2 prepared from titanium tetrachloride and titanium tetraisopropoxide. Materials Chemistry and Physics, 133, 304-310.

[3238] Lutterotti L. (2017) MAUD - Materials Analysis Using Diffraction http://maud.radiographema.com/. Accessed May 2017.

[3339] Shirley, D.A., (1972). High-Resolution X-Ray Photoemission Spectrum of the Valence Bands of Gold. Physical Review B: Condensed Matter, 5, 4709-4713.

[3440] Moulder, J.F., Stickle, W.F., Sobol, P.E., Bomben, K.D. (1992). In J. Chastain (Ed.), Handbook of X-ray Photoelectron Spectroscopy, Physical Electronics, Perkin-Elmer Corp, Eden Prairie, MN.

[3541] Viana, M.M., Soares, V.F., Mohallem, N.D.S., (2010). Synthesis and characterization of TiO2 nanoparticles. Ceramic International, 36, 2047-2053.

[3642] Gombac, V., De Rogatis, L., Gasparotto, A., Vicario, G., Montini, T., Barreca, D., Balducci, G., Fornasiero, P., Tondello, E., Graziani, M., (2007). TiO2 nanopowders doped with boron and nitrogen for photocatalytic application. Chemical Physics., 339, 111-123.

[3743] Xu, J., Ao, Y., Chen, M., Fu, D., (2009). Low temperature preparation of boron-doped titania by hydrothermal method and its photocatalytic activity. Journal of. Alloys and Compdounds, 484, 73-79.

[3844] Tobaldi, D.M., Gao, L., Gualtieri, A.F., Sever Skapin, A., Tucci, A., Giacobbe, C., (2012). Mineralogical and optical characterization of SiO2-, N-, and SiO2/N-co-doped titania nanopowders. Journal of American Ceramic Society, 95, 1709-1716.

[3945] Di Paola, A., Bellardita, M., Palmisano, L., (2013). Brookite, the least known TiO2 photocatalyst. Catalysts, 3, 36-73.

[4046] NIST Chemistry WebBook, Gaithersburg, Md/Boulder, Colo, http://srdata. nist.gov/. Accessed May 2017.

[4147] Han, C., Pelaez, M., Likodimos, V., Kontos, A.G., Falaras, P., O'Shea, K., Dionysiou, D.D., (2011). Innovative visible light-activated sulfur doped TiO2 films for water treatment. Applied Catalysis B: Environmental, 107, 77-87.

[4248] Colon, G., Hidalgo, M.C., Munuera, G., Ferino, I., Cutrufello, M.G., Navio, J.A., (2006). Structural and surface approach to the enhanced photocatalytic activity od sulfated TiO2 photocatalyst. Applied Catalysis B: Environmental, 63, 45-59.

[4349] Gomathi Devi, L., Kavitha, R., (2014). Enhanced photocatalytic activity of sulfur doped TiO2 for the decomposition of phenol: a new insight into the bulk and surface modification. Material Chemistry and Physics, 143, 1300-1308.

[4450] Ohno, T., Akiyoshi, M., Umebayashi, T., Asai, K., Mitsui, T., Matsumura, M., (2004). Preparation of S-doped TiO2 photocatalysts and their photocatalytic activities under visible light. Applied Catalysis A: General, 265, 115-121.

[4551] Nanayakkara, C.E., Pettibone, J., Grassian, V.H., (2012). Sulfur dioxide adsorption and photooxidation on isotopically-labeled titanium dioxide nanoparticle surfaces: roles of surface hydroxyl groups and adsorbed water in the formation and stability of adsorbed sulfite and sulfate. Physical Chemistry Chemical Physics, 14, 6957-6966.

[4652] Topalian, Z.,. Niklasson, G.A , Granqvist, C.G., Osterlund, L., (2012). Spectroscopic study of the photofixation of SO2 on anatase TiO2 thin films and their oleophobic properties. Applied Materials and Interfaces, 4, 672-679.

[47] Sahoo, C., Gupta, A.K., Pal, A., (2005). Photocatalytic degradation of methyl red dye in aqueous solutions under UV irradiation using Ag^{+} doped TiO2. Desalination, 181, 91-100.

[48] Badr, Y., Abd El-Wahed, M.G., Mahmoud, M.A., (2008). Photocatalytic degradation of methyl red dye by silica nanoparticles. Journal of. Hazardous Materials, 154, 245-253.

[49] Lachheb, H., Puzenat, E., Houas, A., Ksibi, M., Elakoui, E., Guillard, C., Herrmann, J.M., (2002). Photocatalytic degradation of various types of dyes (Alizarin S, Crocein OrangeG, Methyl Red, Congo Red, Methylene Blue) in water by UV-irradiated titania. Applied Catalysis B: Environmental, 39, 75-90.

[5053] Lopez-Munoz, M.J., Revilla, A., Alcalde, G., (2015). Brookite TiO2-based materials: synthesis and photocatalytic performance in oxidation of methyl orange and As(III) in aqueous suspensions. Catalysis Today, 240, 138-145.

[5154] Comparelli, R., Fanizza, E., Curri, M.L., Cozzoli, P.D., Mascolo, G., Passino, R., Agostiniano, A., (2005). Photocatalytic degradation of azo dyes by organic-capped anatase TiO2 nanocrystals immobilized onto substrates. Applied Catalysis B: Environmental, 55, 81-91.

[5255] Comparelli, R.: Fanizza, E., Curri, M.L., Cozzoli, P.D., Mascolo, G., Agostiniano, A., (2005). UV-induced photocatalytic degradation of azo dyes by organic-capped ZnO nanocrystals immobilized onto substrates. Applied Catalysis B: Environmental, 60, 1-11.

[5356] Mascolo, G., Comparelli, R., Curri, M.L., Lovecchio, G., Lopez, A., Agostiniano, A., (2007). Photocatalytic degradation of methyl red by TiO2: comparison of the efficiency of immobilized nanoparticles versus conventional suspended catalyst. Journal of. Hazardous Materials, 142, 130-137.

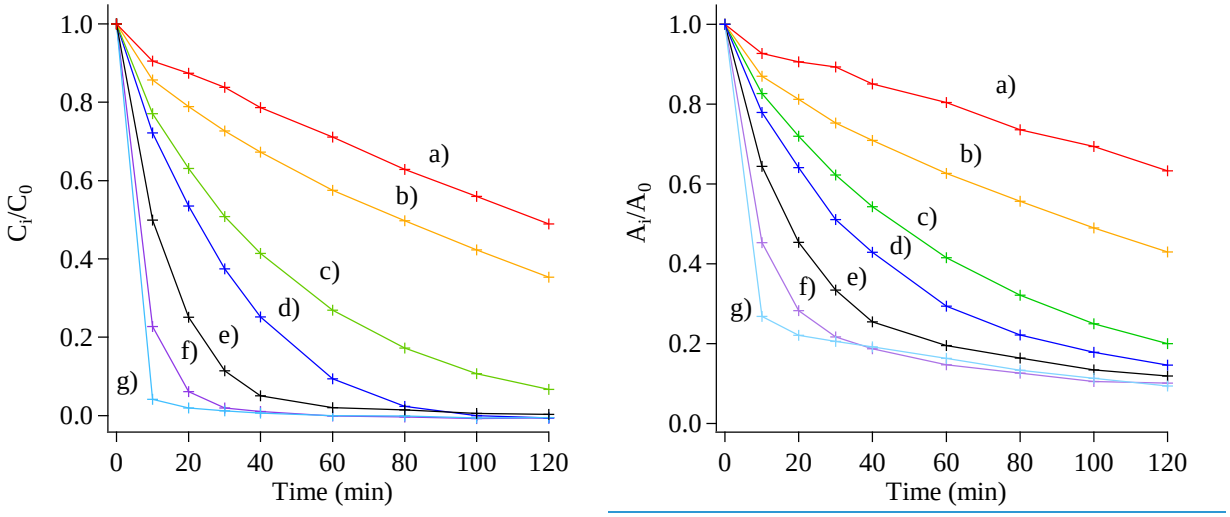

Figure 6. a) MR concentration profiles (normalised with respect to the initial concentration C_0), b) area of the region bounded by the UV-Vis spectra (normalised with respect to the initial area) as a function of reaction time for the investigated samples at pH 2: (a) r-TiO_2 (red), (b) TiO_2-W1 (orange), (c) TiO_2-W2 (green), (d) TiO_2 (blue), (e) a-TiO_2 (black), (f) P25 (purple), (g) S-TiO_2 (light blue).

Table 1. XRD composition, crystallite sizes, BET specific surface area and band gap energy obtained for the investigated samples.

[a] The more the goodness of fitting approaches the unity, the better the fitting quality turns out to be.

Sample	Phase(s) and relative wt %	Crystallite size (nm)	Goodness of fitting [a]	ICDD card	BET surface area (m^2/g)	Band gap (eV)
r-TiO_2	Rutile (100)	275	1.32	01-089-4920	0.4	3.0
TiO_2-W1	Rutile (100)	10	1.35	01-089-4920	143.8	3.1
a-TiO_2	Anatase (100)	25	1.01	01-084-1286	83.1	3.1
TiO_2-W2	Brookite (56) Rutile (34) Anatase (10)	20 30 10	1.12	00-015-0875 01-089-4920 01-084-1286	70.6	3.0
TiO_2	Anatase (77) Rutile (23)	30 50	1.13	01-084-1286 01-089-4920	85.8	3.0
S-TiO_2	Anatase (63) Rutile (37)	15 15	1.21	01-084-1286 01-089-4920	123.7	3.0
P25	Rutile (~~91~~9) Anatase (9~~9~~1)	60 40	1.20	01-089-4920 01-084-1286	50.5	3.0

Table 2 Methyl red conversions and residual areas after 10, 30 and 120 minutes of reaction and first order kinetic constant values (with respect to the MR disappearance) obtained in photocatalytic test at pH 2.

Sample	MR Conversion at 10 - 30 - 120' (%)	Residual area at 10 - 30 - 120' (%)	k (min^{-1})
r-TiO_2	9.5 - 16.2 - 51.1	92.7 - 89.3 - 63.3	0.006
TiO_2-W1	14.3 - 27.3 - 64.7	87.0 - 75.3 - 43.0	0.009
a-TiO_2	50.1 - 88.6 - 99.7	64.6 - 33.4 - 11.9	0.070
TiO_2-W2	22.9 - 49.2 - 93.3	82.7 - 62.3 - 20.0	0.023
TiO_2	27.8 - 62.5 - 100.0	77.9 - 51.1 - 14.6	0.038
S-TiO_2	95.9 - 98.8 - 100.0	26.8 - 20.6 - 9.4	0.310
P25	77.3 - 98.1 - 100.0	45.3 - 21.7 - 10.1	0.151